

Electromagnetic Follow-up Observations of Binary Neutron Star Mergers with Early Warnings from Decihertz Gravitational-wave Observatories

Yacheng Kang,^{1,2} Chang Liu,^{1,2} and Lijing Shao^{2,3}★

¹Department of Astronomy, School of Physics, Peking University, Beijing 100871, China

²Kavli Institute for Astronomy and Astrophysics, Peking University, Beijing 100871, China

³National Astronomical Observatories, Chinese Academy of Sciences, Beijing 100012, China

Accepted XXX. Received YYY; in original form ZZZ

ABSTRACT

We investigate the prospects of electromagnetic follow-up observations for binary neutron star (BNS) mergers, with the help of early warnings from decihertz gravitational-wave (GW) observatories, B-DECIGO and DO-Optimal. Extending the previous work, we not only give quick assessments of joint short γ -ray burst (sGRB) detection rates for different γ -ray satellites and BNS population models, but also elaborate on the analyses and results on multi-band kilonova detections for survey telescopes with different limiting magnitudes. During an assumed 4-year mission time for decihertz GW observatories, we find that for the goals of electromagnetic follow-ups, DO-Optimal performs better than B-DECIGO as a whole on the detection rate, and has a larger detectable distance for joint sGRB/kilonova searches. Taking the log-normal population model for BNS mergers and a one-day early-warning time as an example, we discuss the accuracy in localization and timing, as well as the redshift distributions for various synergy observations with electromagnetic facilities and decihertz GW detectors. Based on our analyses, we propose a feasible “wait-for” pattern as a novel detecting mode for future multi-messenger astrophysics.

Key words: gravitational waves – neutron star mergers – gamma-ray bursts

1 INTRODUCTION

The first binary neutron star (BNS) merger, GW170817, was initially alerted by the advanced LIGO and Virgo detectors (Abbott et al. 2017a), and the gravitational wave (GW) signal was followed up by intensive observations across the whole electromagnetic (EM) spectrum (Abbott et al. 2017b). Because of this, GW170817 marks a spectacular success of multi-messenger astrophysics, and has been viewed as the watershed moment in astronomy and physics (Kalogera et al. 2021). From the combination of GW and EM data, its luminosity distance is determined to be $D_L \approx 40$ Mpc (Hjorth et al. 2017). Thanks to the short distance, GW170817 has been subsequently confirmed in association with a short γ -ray burst (sGRB) ~ 1.7 s after the merger (GRB 170817A; Abbott et al. 2017c; Goldstein et al. 2017; Savchenko et al. 2017; Zhang et al. 2018), a kilonova discovered in the galaxy NGC 4993 ~ 11 hr later (AT 2017gfo; Coulter et al. 2017; Evans et al. 2017; Pian et al. 2017; Kilpatrick et al. 2017), and an off-axis multi-wavelength afterglow detected with its luminosity peaking at ~ 200 d (Margutti et al. 2017; Troja et al. 2017; Lazzati et al. 2018; Lyman et al. 2018; Ghirlanda et al. 2019). Such a multi-messenger observation has not only provided us the smoking-gun evidence for the BNS merger origin of sGRBs and kilonovae (Abbott et al. 2017c; Li & Paczynski 1998), but also an unprecedented opportunity to explore dense matter properties and gravity theories in extreme environments (Abbott et al. 2017d, 2018, 2019a). These aspects are vital to many open questions in the fundamental physics (Sathyaprakash et al. 2019; Arun et al. 2022).

However, in addition to GW170817, there is only one other potentially heavy BNS merger event to date in the LIGO/Virgo/KAGRA data (GW190425; Abbott et al. 2020). The fast-evolving nature of sGRBs and kilonovae might appear discouraging for multi-messenger observations after the BNS mergers (Zhu et al. 2021a), let alone the common faintness for current EM follow-up facilities due to the large distances between most BNS mergers and the Earth (Zhu et al. 2021b). Owing to many difficulties for all-sky multi-messenger detections of BNS mergers using the traditional time-domain survey projects, some studies have been devoted to the best searching strategy with ground-based GW triggers for EM follow-up observations (Cowperthwaite & Berger 2015; Gehrels et al. 2016; Rosswog et al. 2017; Cowperthwaite et al. 2019; Liu et al. 2022b), especially focusing on kilonova detections by serendipitous observations (Metzger & Berger 2012; Coughlin et al. 2017, 2020b; Zhu et al. 2021c,b). What were discussed in these studies have included different proposals for present and future GW/EM synergy projects, characterized by the field of view (FoV), search cadence, filters, exposure time, and so on. The complexity of these schemes can be overwhelming.

Differently from these former investigations, in this work we discuss the prospects for the multi-messenger observations with GW early warnings using space-borne decihertz GW detectors. As Liu et al. (2022a) recently demonstrated, with decihertz GW detectors alone, the localization and timing accuracy of BNS mergers may achieve a level of $O(0.01)$ deg² and $O(0.1)$ s, respectively. We propose that such results will allow us to prepare a realistic “wait-for” pattern for various γ -ray satellites and survey telescopes with current or future designs, even in the case that we request a one-day early-warning time before the BNS merger. By contrast, current and future

★ E-mail: lshao@pku.edu.cn

ground-based GW detectors can not provide localization estimates as accurately as the space-borne decihertz GW detectors (Magee & Borhanian 2022; Borhanian & Sathyaprakash 2022). Due to the higher sensitive frequency range of the ground-based detectors, they can not offer alerts as early as the decihertz GW detectors, either. Without a sufficient early-warning time, it is also hard for EM telescopes to capture the early evolution of each detectable BNS merger, even for the low-latency GW-trigger events. EM follow-up facilities usually need response time to make decisions and tune satellites and telescopes. Nevertheless, our results on the EM follow-up observations of BNS mergers with space-borne decihertz GW detectors will bring excellent opportunities for future multi-messenger astronomy.

We study a wait-for scheme with four BNS population models and two representative decihertz GW detectors, B-DECIGO (B-DEC; Isoyama et al. 2018; Kawamura et al. 2021) and DO-Optimal (DO-OPT; Sedda et al. 2020). Taking the log-normal population model for BNS mergers and a one-day early-warning time as an example, our results show that both B-DEC and DO-OPT can reach a localization accuracy of $\Delta\Omega \lesssim 1 \text{ deg}^2$ and timing accuracy of $\Delta t_c \lesssim 0.5 \text{ s}$. This will be of great use to synergy observations with EM facilities. We also find that DO-OPT is expected to have a better performance than B-DEC as a whole on the joint sGRB/kilonova detection rate, especially for the high-redshift events. With the redshift distributions for sGRB/kilonova searches presented in this work, we provide meaningful references and helpful inputs for upcoming EM follow-up projects. We admit that a specific ground-based optical survey mission should consider the discount due to its maximum detectable sky coverage and the Earth’s rotation. But this can be partially solved if there are at least two survey telescopes on the different sides of the Earth. More importantly, due to the accurate localization and timing ability of decihertz GW detectors with a sufficient early-warning time in our scenario, there is no need to consider a complex searching strategy for the EM follow-up observations anymore. Such a wait-for pattern could also provide a rare opportunity for analyzing the early evolution characteristics of each detectable system, which we leave to future studies.

The organization of this paper is as follows. Following the method and procedure presented in Liu et al. (2022a), in Sec. 2 we first overview the BNS merger populations and the GW detecting strategy with two space-borne decihertz GW observatories. For EM follow-up observations, we present our methodologies on the sGRB and kilonova detections in Sec. 3. Using the above ingredients, we report detailed analyses and results on various aspects of multi-messenger early-warning detections in Sec. 4. Finally, Sec. 5 concludes the paper. We use geometric units where $G = c = 1$.

2 GW EARLY WARNINGS OF BNS MERGERS

As mentioned in the Introduction, one major difference between our work and other researches on multi-messenger observations of BNS mergers is that we aim to explore how to achieve the wait-for pattern for various EM facilities with the early warnings from decihertz GW detectors. Therefore, in this section, we briefly overview the early-warning populations for later analyses.

Before quantitatively analyzing the early warnings from GW observatories and the EM counterparts from BNS mergers, one needs to obtain their redshift distributions in our Universe. Given that there are various types of population models in literature and their predicted results vary widely among different models, especially for the high-redshift regime, we follow Liu et al. (2022a) and consider four kinds

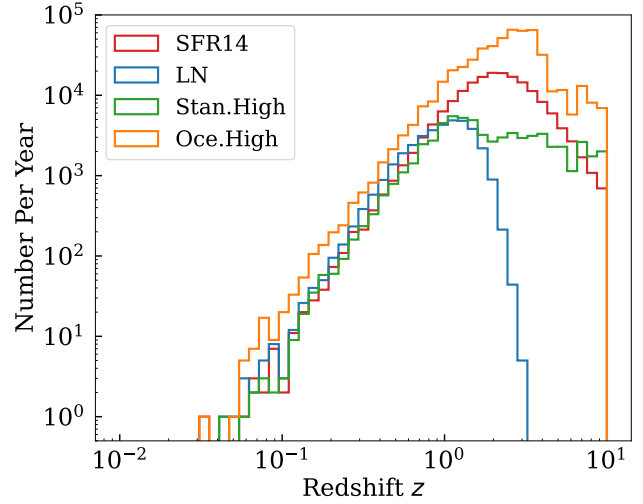


Figure 1. Total number of BNS mergers per year for different population models.

of population models. The models—abbreviated as “SFR14”, “LN”, “Stan.High”, and “Oce.High”—are briefly summarized as follows:

- (1) **SFR14**—BNS merger rate evolves with redshift following the fitting formula of star formation rate (SFR) in Madau & Dickinson (2014);
- (2) **LN**—We consider the log-normal delay model based on a delay time superposed on the SFR (Wanderman & Piran 2015; Sun et al. 2015; Zhu et al. 2021c);
- (3) **Stan.High**—We adopt the standard model with high-end metallicity evolution scenarios from Dominik et al. (2013);
- (4) **Oce.High**—We adopt the optimistic common envelope model with high-end metallicity evolution scenarios from Dominik et al. (2013).

Based on the GWTC-3 PDB (ind) model (Abbott et al. 2021), we adopt the local merger rate $44 \text{ Gpc}^{-3} \text{ yr}^{-1}$ for BNSs. The redshift cutoff is at $z \approx 10$ and more details about BNS populations can be found in Liu et al. (2022a). Note that a standard Λ CDM cosmology with $H_0 = 67.8 \text{ km s}^{-1} \text{ Mpc}^{-1}$, $\Omega_\Lambda = 0.692$, and $\Omega_m = 0.308$ is assumed in this work (Ade et al. 2016). Finally, we plot the distributions of BNS mergers in Fig. 1 for the above population models.¹

For each BNS, their NS masses, M_1 and M_2 , are randomly generated based on the observational distribution of Galactic BNS systems, using a normal distribution $M_{1,2}/M_\odot \sim \mathcal{N}(1.32, 0.11^2)$ for each NS (Lattimer 2012; Kiziltan et al. 2013). This distribution has been adopted in other studies as well (Song et al. 2019; Yu et al. 2021; Zhu et al. 2021b). With known $M_{1,2}$ and redshift z , we will discuss the prospects for multi-messenger early-warning detections of BNS mergers in the following sections.

For multi-messenger detections of BNS mergers, the space-borne decihertz GW detectors could offer alerts much earlier than ground GW detectors and EM facilities. We report detailed analyses with

¹ In a recent paper, O’Connor et al. (2022) have suggested that a power-law delay time distribution with a decay index between ~ -1 and -1.5 seems to be consistent with the deeper observational results. If this is confirmed, we caution that the LN model might underestimate the rate of high- z events.

early warnings only from B-DEC and DO-OPT for in-depth comparisons. Conservatively, we set a 4-yr mission time for the two decihertz GW detectors in our work. More detailed descriptions of these detectors are presented in, e.g., [Liu & Shao \(2022\)](#).

Recently, [Liu et al. \(2022a\)](#) have classified all BNS mergers in decihertz GW detectors into 3 categories based on the observational properties, in particular the accuracy of angular resolution $\Delta\Omega$ and time of merger Δt_c . Three categories are:

- (a) BNSs that merge within 1 year since the start of observation ($t_{c_0} \leq 1$ yr);
- (b) BNSs that merge in 1 to 4 years ($1 \text{ yr} < t_{c_0} \leq 4 \text{ yr}$);
- (c) BNSs that only inspiral within the whole 4-yr observational span ($t_{c_0} > 4 \text{ yr}$).

Here t_{c_0} is defined as the merger time since the mission begins. For sources in category (a), due to their short stay in the decihertz detector, not enough information could be accumulated to obtain precise parameter estimations. As an example, the angular resolution for B-DEC could reach $O(10^4) \text{ deg}^2$, which may not be covered by the FoV of EM telescopes, let alone for the wait-for pattern discussed in this work. For mergers in category (c), although space-borne decihertz detectors could provide warnings much earlier than the ground facilities, their timing accuracies have shown a sharp decreasing trend ([Liu et al. 2022a](#)), which is unfavorable for multi-messenger early-warning detections. Furthermore, their detection results do not play a major part in our simulations for both two GW detectors. Therefore, we only use the early-warning BNS merger samples in category (b). Those events not only make up the majority of the total BNS mergers but also yield the best and most stable estimation results.

Following [Liu et al. \(2022a\)](#), we use the Fisher information matrix to estimate 9 system parameters, collectively denoted as $\Xi = \{\mathcal{M}, \eta, t_c, \phi_c, D_L, \theta_S, \bar{\phi}_S, \bar{\theta}_L, \bar{\phi}_L\}$, to obtain the parameter precisions of each event. In Ξ , $\eta \equiv M_1 M_2 / (M_1 + M_2)^2$ is the symmetric mass ratio; $\mathcal{M} \equiv (M_1 + M_2) \eta^{3/5}$ is the chirp mass; t_c and ϕ_c are the time and orbital phase at coalescence, respectively; and $\{\bar{\theta}_S, \bar{\phi}_S, \bar{\theta}_L, \bar{\phi}_L\}$ are the source direction and angular momentum direction in the Solar system barycentric frame (see Fig. 1 in [Liu et al. 2020](#)). From $\{\bar{\theta}_S, \bar{\phi}_S, \bar{\theta}_L, \bar{\phi}_L\}$ we can obtain the viewing angle θ_{obs} in the next section. The signal-to-noise ratio (SNR) threshold is set to be 8 in this work. Our attention focuses on the estimation of the accuracy of angular resolution $\Delta\Omega$ and time of merger Δt_c . For the Fisher matrix in the frequency domain, we set the integration limit to be f_{in} and f_{out} . As a BNS is to merge in time t_{c_0} , we have $f_{\text{in}} = (t_{c_0}/5)^{-3/8} \mathcal{M}^{-5/8}/8\pi$ and $f_{\text{out}} = (t_e/5)^{-3/8} \mathcal{M}^{-5/8}/8\pi$ with t_e representing the early-warning time before the merger. The early-warning time t_e is remarkably significant to the multi-messenger early-warning detections of BNS mergers. We mainly present the results with $t_e = 1 \text{ d}$ in detail, and analyses with a larger t_e will be briefly mentioned.

3 EM COUNTERPART DETECTION

Based on the GW early-warning populations, we explore the multi-messenger observations with the multi-band EM follow-ups. Following [Song et al. \(2019\)](#) and [Yu et al. \(2021\)](#), in Sec. 3.1 we first briefly introduce the method of sGRB detections, which are expected to occur shortly after the BNS mergers. Compared to the kilonovae, there have already been many cosmological sGRB afterglows observed ranging from radio to X-rays to date ([Zhang 2018](#)). Thus in Sec. 3.2 we focus on the early-warning kilonova detections and report our results with detailed analyses.

Table 1. Parameters of GRB 170817A afterglow using Gaussian jet model ([Ryan et al. 2020](#)).

Parameter	Value
θ_c/rad	$0.066^{+0.018}_{-0.018}$
θ_w/rad	$0.47^{+0.26}_{-0.19}$
$\log_{10}(E_0/\text{erg})$	$52.96^{+0.97}_{-0.72}$
$\log_{10}(n_0/\text{cm}^{-3})$	$-2.7^{+1.0}_{-1.0}$
p	$2.1675^{+0.0063}_{-0.0075}$
$\log_{10} \epsilon_e$	$-1.4^{+0.7}_{-1.1}$
$\log_{10} \epsilon_B$	$-4.0^{+1.1}_{-0.7}$

Note. n_0 is the circumburst density; p is the electron energy index; ϵ_e and ϵ_B are the fractions of shock energy carried by electrons and magnetic fields, respectively. The given posterior values are the medians, along with their 16%, and 84% quantiles.

3.1 sGRB Detection

The observational fact that GRB 170817A is abnormally less energetic than typical sGRBs ([Goldstein et al. 2017](#); [Zhang et al. 2018](#)) with the slowly rising multi-band light curves ([Troja et al. 2017, 2018](#); [Lazzati et al. 2018](#); [Lyman et al. 2018](#); [Mooley et al. 2018](#)) suggested that the scenario of BNS merger is most likely to be an off-axis configuration ([Rossi et al. 2002](#); [Zhang & Mészáros 2002](#)). Among a variety of jet energy profiles, we adopt the Gaussian structured jet model ([Zhang & Mészáros 2002](#)),

$$E(\theta) = E_0 \exp\left(-\frac{\theta_{\text{obs}}^2}{2\theta_c^2}\right), \quad \theta_{\text{obs}} \leq \theta_w, \quad (1)$$

where E_0 is the on-axis equivalent isotropic energy, θ_{obs} is the polar viewing angle, θ_c is the characteristic core angle, and θ_w is the truncation angle of the jet, which means that the energy would be initially zero for $\theta_{\text{obs}} > \theta_w$. This model is favored by former analyses ([Lazzati et al. 2018](#); [Mooley et al. 2018](#); [Troja et al. 2018, 2019a, 2020](#); [Xie et al. 2018](#); [Lamb et al. 2019](#)). [Ryan et al. \(2020\)](#) has given the constraints on the jet and afterglow parameters for GRB 170817A, which are listed in Table 1. Throughout this paper, all the parameters in Table 1 are fixed to their median values for simplification.

Following [Yu et al. \(2021\)](#), we assume that every early-warning BNS merger event in our simulation is associated with an sGRB, whose jet profile is broadly similar to that of GRB 170817A in Eq. (1). Assuming that the burst duration $T_{90} \sim 2 \text{ s}$ ([Abbott et al. 2017b](#)) and the spectrum is flat with time during T_{90} , the γ -band flux for each BNS merger is,

$$F_\gamma = \frac{E_0 \eta_\gamma}{4\pi D_L^2 T_{90}} \exp\left(-\frac{\theta_{\text{obs}}^2}{2\theta_c^2}\right), \quad \theta \leq \theta_w, \quad (2)$$

where η_γ is the radiative efficiency and we use $\eta_\gamma \sim 0.1$ for the bolometric energy flux in the $1\text{--}10^4 \text{ keV}$ band ([Yu et al. 2021](#)). For all BNS-associated sGRBs, we assume that the γ -ray spectrum is described by the Band function with photon indices $\alpha = -1$ and $\beta = -2.3$ respectively below and above the peak energy E_p in the νF_ν spectra ([Preece et al. 2000](#)). Note that E_p changes with θ_{obs} via

Table 2. Summary of technical information for each proposed survey from Zhu et al. (2021b,c) and CSST-HOD, assuming a 300-s exposure time for the search limiting magnitude m^* .

Telescope	m^*			FoV/deg ²	Reference
	g	r	i		
WFST	24.18	23.95	23.33	6.55	Shi et al. (2018)
LSST	26.15	25.70	25.79	9.6	Abell et al. (2009)
CSST	26.3	26.0	25.9	1.1	Gong et al. (2019)
CSST-HOD	27	27	27	—	—

the relationship proposed by Ioka & Nakamura (2019) to make the GRB 170817A observation consistent with previous sGRB data via,

$$E_p(\theta_{\text{obs}}) = E_{p,0} (1 + \theta_{\text{obs}}/\theta_c)^{-0.4}, \quad (3)$$

where $E_{p,0}$ can be calculated by the Yonetoku relation (Yonetoku et al. 2004) with the central luminosity of the Gaussian jet.

Adopting the same setting of four γ -ray detectors as in Yu et al. (2021), the sensitivity for the Fermi Gamma-ray Burst Monitor (Fermi-GBM) is $\sim 2 \times 10^{-7} \text{ erg s}^{-1} \text{ cm}^{-2}$ in the 50–300 keV band (Meegan et al. 2009); the sensitivity for the Gravitational wave high-energy Electromagnetic Counterpart All-sky Monitor (GECAM) is $\sim 1 \times 10^{-7} \text{ erg s}^{-1} \text{ cm}^{-2}$ in the 50–300 keV band (Zhang et al. 2019); the sensitivity for the Swift Burst Alert Telescope (BAT) and the Space Variable Objects Monitor (SVOM)-ECLAIRS is $\sim 1.2 \times 10^{-8} \text{ erg s}^{-1} \text{ cm}^{-2}$ in the 15–150 keV band (Gehrels et al. 2004; Lien et al. 2014; Götz et al. 2015). Based on the above assumptions, we can obtain the effective sensitivity limit for different γ -ray detectors in the 1–10⁴ keV band. By comparing F_γ with the effective sensitivity limit, we can then assess whether the simulated sGRB could be detected by a specific γ -ray detector. As shown in Fig. 2 of Song et al. (2019), the effective sensitivity for Swift-BAT and SVOM-ECLAIRS (denoted as “SBSE” hereafter) performs the best in the 1–10⁴ keV band, while Fermi-GBM (denoted as “FG” hereafter) has the worst performance. Although these γ -ray detectors might have no overlapping observational time with our space-borne decihertz GW observatories (B-DEC and DO-OPT), our results can still apply to the similar detectors at that time. Furthermore, for each detector mentioned above, we also have considered hypothetically optimized devices (HODs). We artificially set their sensitivities to be one (HOD-1) and two (HOD-2) orders of magnitude better than the current ones. The results on the sGRB detections are given in Sec. 4.

3.2 Kilonova Detection

Li & Paczynski (1998) predicted thermal, supernova-like transients with a duration of a day to a week after BNS mergers. Since then the kilonova provides both a candidate EM counterpart to the GW-triggered BNS mergers and a probe of the astrophysical origin of r -process elements (Metzger et al. 2010; Metzger 2017). However, it can be difficult to detect the cosmological kilonovae not associated with beamed sGRBs and afterglows due to their relatively low luminosity and fast-evolving nature. In addition to AT 2017gfo with relatively complete observations of kilonova properties, there is no kilonova candidate for the third observing run (O3) of LIGO/Virgo/KAGRA (Kasliwal et al. 2020; Becerra et al. 2021; de Jaeger et al. 2021; Dichiaro et al. 2021; Mohite et al. 2022). Therefore, following Zhu et al. (2021a), we simply assume that all kilono-

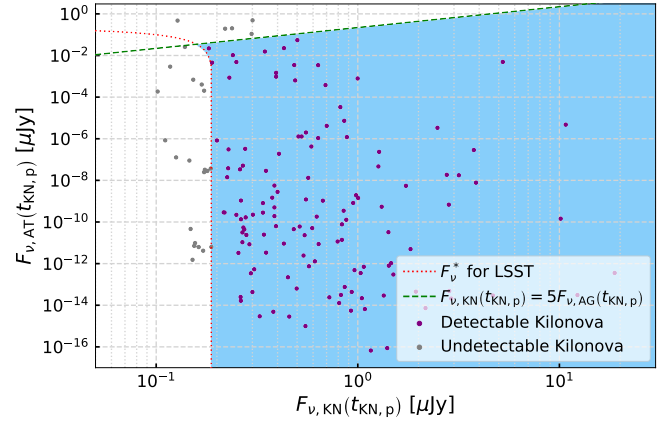


Figure 2. Kilonova detection parameter space for r -band of LSST. The shaded blue region delimits the detectable $F_{v,KN}$ – $F_{v,AG}$ space according to the two criteria in the main text. The GW early-warning kilonovae in this figure are obtained from B-DEC with $2 \text{ yr} < t_{c0} \leq 3 \text{ yr}$, assuming the LN population model and $t_e = 1 \text{ d}$.

vae are AT 2017gfo-like in view of the scarce data to date.² Adopting the model generated by the POSSIS package (Bulla 2019; Coughlin et al. 2020a), which considered a polar-dominated lanthanide-free (LF) component and an equatorial-dominated lanthanide-rich (LR) component with different opacities, we can obtain the multi-band kilonova data with a total ejecta mass $M_{\text{ej}} = 0.04 M_\odot$ and a half-opening angle of the LR component $\Phi = 60^\circ$ (for example, see Fig. 2 in Zhu et al. 2021a).

The presence of relatively bright jet afterglows may affect observations of kilonovae for on-axis or near-axis observers. Therefore, we define a detectable kilonova event with two criteria (Zhu et al. 2021b),

- (i) $F_{v,KN}(t_{KN,p}) + F_{v,AG}(t_{KN,p}) > F_v^*$, and
- (ii) $F_{v,KN}(t_{KN,p}) > 5F_{v,AG}(t_{KN,p})$,

where $t_{KN,p}$ is the peak time of the kilonova; $F_{v,KN}$ and $F_{v,AG}$ are the peak kilonova flux and the afterglow flux, respectively; F_v^* is

² Note that there are many theoretical works suggesting that BNS kilonovae should be diverse, depending on the mass ratio of the binary and the nature of the merger remnant (Kasen et al. 2013, 2017; Kawaguchi et al. 2020, 2021; Korobkin et al. 2021). Also, some recent observational data have shown evidence for the deviations from AT 2017gfo (Tanvir et al. 2013; Troja et al. 2019b; O’Connor et al. 2021). In view of this, we caution that some results in this paper can be affected by the diversity of the kilonovae. A future dedicated investigation is required to address this aspect fully.

Table 3. Yearly joint GW-sGRB detection numbers and percentages observed by different γ -ray missions and two decihertz GW detectors for different early-warning BNS merger populations. We assume an early-warning time $t_e = 1$ d. We list the total number of early-warning BNS mergers per year in the parentheses below B-DEC and DO-OPT, which are used in the percentage calculations. In each cell we list the result with the current design for each γ -ray detector as the first entry, and present results for HOD-1 and HOD-2 as the second and the third entries. These values are separated by two slashes.

Population	Detector	FG	GECAM	SBSE
LN	B-DEC (166)	5 / 12 / 19 (3.0 % / 7.2 % / 11 %)	6 / 15 / 20 (3.6 % / 9.0 % / 12 %)	10 / 19 / 25 (6.0 % / 11 % / 15 %)
	DO-OPT (1.3×10^4)	10 / 158 / 465 (<0.1 % / 1.3 % / 3.7 %)	28 / 243 / 554 (0.2 % / 1.9 % / 4.4 %)	120 / 428 / 736 (1.0 % / 3.4 % / 5.9 %)
SFR14	B-DEC (127)	3 / 7 / 14 (2.4 % / 5.5 % / 11 %)	4 / 9 / 14 (3.1 % / 7.1 % / 11 %)	6 / 12 / 16 (4.7 % / 9.4 % / 13 %)
	DO-OPT (1.5×10^4)	10 / 160 / 678 (<0.1 % / 1.1 % / 4.7 %)	22 / 296 / 842 (0.2 % / 2.0 % / 5.8 %)	115 / 622 / 1.2×10^3 (0.8 % / 4.3 % / 8.1 %)
Stan.High	B-DEC (122)	5 / 8 / 12 (4.1 % / 6.6 % / 9.8 %)	6 / 10 / 13 (4.9 % / 8.2 % / 11 %)	7 / 12 / 14 (5.7 % / 9.8 % / 11 %)
	DO-OPT (9.7×10^3)	6 / 118 / 390 (<0.1 % / 1.2 % / 4.0 %)	18 / 198 / 475 (0.2 % / 2.0 % / 4.9 %)	84 / 365 / 661 (0.9 % / 3.8 % / 6.8 %)
Oce.High	B-DEC (332)	9 / 16 / 26 (2.7 % / 4.8 % / 7.8 %)	10 / 20 / 29 (3.0 % / 6.0 % / 8.7 %)	14 / 24 / 35 (4.2 % / 7.2 % / 11 %)
	DO-OPT (3.3×10^4)	17 / 342 / 1.5×10^3 (<0.1 % / 1.0 % / 4.5 %)	44 / 642 / 1.8×10^3 (0.1 % / 2.0 % / 5.6 %)	234 / 1.4×10^3 / 2.6×10^3 (0.7 % / 4.1 % / 7.8 %)

the effective limiting flux for different survey telescopes. Three proposed survey projects with three most common filters (*gri*) have been considered in our work, which are the Wide Field Survey Telescope (WFST; [Shi et al. 2018](#)), the Large Synoptic Survey Telescope (LSST, newly named as the Vera Rubin Observatory; [Abell et al. 2009](#)), and the Chinese Space Station Telescope (CSST; [Gong et al. 2019](#)). Some technical parameters for these proposed survey telescopes are given in Table 2. We could obtain $F_\nu^* \simeq 3631 \text{ Jy} \times 10^{-m^*/2.5}$ in each band when the search limiting magnitude m^* is given. Note that a 300-s exposure time is adopted throughout this paper and we again consider a HOD for CSST (CSST-HOD) with one magnitude better sensitivity than CSST in each band (see Table 2).

Taking the LN population model with $t_e = 1$ d for B-DEC as an example, we plot in Fig. 2 the selection functions corresponding to the criteria (i) and (ii) above. The red dotted line corresponds to the r -band effective limiting flux F_ν^* of LSST, and the green dashed line indicates the boundary of criterion (ii). Therefore, the shaded blue region in Fig. 2 delimits the detectable $F_{\nu, \text{KN}} - F_{\nu, \text{AG}}$ parameter space of kilonovae for LSST.

For all the valuable early-warning joint GW-kilonova observations, we further classify them into two groups, “*GK*” and “*K*”, based on the observation of sGRB and kilonova, according to

- (I) *GK*: both sGRB and kilonova can be detected;
- (II) *K*: kilonova can be detected while sGRB cannot.

Here we mention that, observing *K* samples is indeed significant, but

without the synergy with sGRB as *GK* samples, sometimes it can be difficult to distinguish kilonovae from other rapid-evolving transients, for example, some supernova events ([Mazzali et al. 2008](#); [Prentice et al. 2018](#); [Perley et al. 2019](#); [McBrien et al. 2019](#); [Chen et al. 2020](#)). Therefore, more attention should be paid to the *GK* samples in future work. In this work we use *afterglowpy*, an open-source Python package ([Ryan et al. 2020](#)), to model the light curves of multi-wavelength afterglow and obtain the $F_{\nu, \text{AG}}$ value with parameters listed in Table 1. Note that for *GK* and *K* samples, the definition of sGRB detection is based on the detection result of SBSE, except for CSST-HOD. We consider the SBSE-HOD-1 and CSST-HOD to achieve more cooperative observations during the same period.

4 RESULTS

Now we give detailed results for the multi-messenger early-warning detections of BNS mergers. Given that the merger events in our consideration from category (b) with $1 \text{ yr} < t_{c0} \leq 4 \text{ yr}$ are in general distributed uniformly in time (see e.g., Fig. 3 and Fig. 7 in [Liu et al. 2022a](#)), we divide the total GW early-warning events by 3 and present the yearly sGRB and kilonova detection rates in Sec. 4.1. In Sec. 4.2, we plot the characteristic distributions of the yearly multi-messenger events. Note that for all the scatter plots, we choose the early-warning BNS mergers with $2 \text{ yr} < t_{c0} \leq 3 \text{ yr}$.

Table 4. Yearly joint GW-kilonova detection numbers and percentages observed by different survey missions and two decihertz GW detectors for our early-warning BNS mergers. We have used the “LN” population model with $t_e = 1$ d as an example. Three values in each cell for *GK* and *K* samples represent the results with *g/r/i* filters. CSST-HOD has approximately one magnitude better sensitivity than CSST (see Table 2 in Sec. 3.2). We have calculated the total number of BNS merger detections, as listed in Table 3 for B-DEC (166) and DO-OPT (1.3×10^4). For WFST and LSST, the 1/4 discount due to the sky coverage Ω_{cov} and the Earth’s rotation is not considered (see Sec. 4.1).

Type	Detector	WFST	LSST	CSST	CSST-HOD
<i>GK</i>	B-DEC	< 1 / 2 / 1 (<0.6 % / 1.2 % / 0.6 %)	3 / 4 / 5 (1.8 % / 2.4 % / 3.0 %)	3 / 4 / 5 (1.8 % / 2.4 % / 3.0 %)	11 / 13 / 14 (6.6 % / 7.8 % / 8.4 %)
		< 1 / 1 / 1 (<0.1 % / <0.1 % / <0.1 %)	2 / 3 / 5 (<0.1 % / <0.1 % / <0.1 %)	2 / 4 / 5 (<0.1 % / <0.1 % / <0.1 %)	12 / 31 / 43 (0.1 % / 0.2 % / 0.3 %)
	DO-OPT	23 / 35 / 30 (14 % / 21 % / 18 %)	111 / 138 / 153 (67 % / 83 % / 92 %)	123 / 150 / 155 (74 % / 90 % / 93 %)	143 / 147 / 147 (86 % / 89 % / 89 %)
		16 / 29 / 22 (0.1 % / 0.2 % / 0.2 %)	181 / 253 / 485 (1.4 % / 2.0 % / 3.9 %)	219 / 361 / 544 (1.7 % / 2.9 % / 4.3 %)	517 / 1.2×10^3 / 1.7×10^3 (4.1 % / 9.4 % / 14 %)

4.1 Detection Rates

As shown in Table 3 we summarize all our simulated joint GW-sGRB detections by different γ -ray missions and two decihertz GW detectors. These results are for different BNS merger populations with an early warning time $t_e = 1$ d. With a GRB 170817A-like Gaussian jet structure, we can see that fewer than 10% of the early-warning BNS mergers for B-DEC would have a γ -band flux higher than the threshold of the γ -ray detectors with current designs. However, with the improved sensitivity by one (two) order(s) of magnitude for each γ -ray detector—namely, HOD-1 (HOD-2) in our notations—we find B-DEC could approximately double (treble) the joint sGRB detection rates, as shown in Table 3. Given that DO-OPT has a lower noise level (see e.g., Fig. 2 in Liu et al. 2022a), we find that it shows better detection abilities, especially for more detections at higher redshift, as we will elaborate later in Sec. 4.2. Furthermore, with a larger t_e , we have verified that the detection rates would decrease due to a shorter stay in the decihertz GW band. For example, all the results could be halved for B-DEC with $t_e = 14$ d.

According to Song et al. (2019), although FG can cover about three-quarters of the whole sky and the FoV for GECAM is about 4π , the FoV/ 4π is $\sim 1/9$ for Swift-BAT and $\sim 1/5$ for SVOM-ECLAIRS, respectively. Considering the short delay between the BNS merger and the sGRB detection, it inevitably means that FoV could become an important discount factor to be reckoned with for joint GW-sGRB detections. However, as we will see later in Sec. 4.2 (e.g., Fig. 3 therein), the sub-deg² localization uncertainty region for decihertz space-borne GW detectors could be totally covered by different γ -ray detectors. Assuming that all the γ -ray satellites are capable of adjusting the pointing to the early-warning BNS mergers, there is no need to consider the discounts from FoVs anymore like previous studies (Song et al. 2019; Yu et al. 2021). We must highlight that with a sufficient t_e prepared for a real sense of early-warning observations, such a wait-for pattern will bring an excellent performance for the joint GW-sGRB detection and future multi-messenger astronomy.

On the other hand, for the early-warning kilonova events, we list the yearly detection results in Table 4 using the LN population model with $t_e = 1$ d as an example. Given a specific combination of GW and EM detectors, we can compare the detection results in different filters (*gri*), as separated by two slashes in the table. Compared with

the results in *g/r*-band, we find that the *i*-band has seen the biggest increase in the proportion of the detection rate from WFST to CSST-HOD, especially for DO-OPT. It can be understood as that more early-warning events will be detected at higher redshift. Considering different m^* values for several optical survey missions in each band, we find that the detection numbers of *K* samples increase remarkably with the improved sensitivity of the survey telescope, while for *GK* samples only CSST-HOD shows obvious improvement compared with the others. The discussion of joint kilonova detections with a hypothetical CSST-HOD is to provide a rough reference for the next-generation survey projects at the same time of decihertz GW detectors.

Again, we assume that the space-borne survey telescopes (CSST and CSST-HOD) can adjust the pointing to each early-warning BNS merger. However, for a specific ground-based optical survey project, the maximum detectable sky coverage Ω_{cov} and the Earth’s rotation must be taken into consideration in the practical kilonova observations. For instance, if the kilonovae are outside Ω_{cov} or occur during the daytime, WFST and LSST may not achieve the early-warning joint GW-kilonova observations, even though we have a sufficient t_e for it. The $\Omega_{\text{cov}}/4\pi$ is $\sim 1/2$ for both WFST and LSST, and we further assume a half-year maximum observation time to provide another 1/2 discount for yearly events. Therefore, in a more realistic situation, we suggest that a factor of 1/4 should be the total discount factor for the results of WFST and LSST in Table 4. Nevertheless, for the wait-for pattern discussed in this work, we also point out that such a discount problem can be partially solved, e.g., with at least two survey telescopes on the different sides of the Earth. Moreover, the long duration of kilonovae (compared with sGRBs) also partially solves this problem. We hope that more studies can be carried out in the future to give more precise predictions with detailed analyses.

Compared with B-DEC in Table 4, we conclude that DO-OPT performs better on the joint GW-kilonova detections as a whole. This is because that DO-OPT can boost the joint kilonova detection rates by detecting more events at higher redshift. We also find some exceptions on the detection numbers, e.g., *K* samples with WFST in Table 4. We suspect that this is attributed to the rounding and random errors in the BNS population simulations, especially for a small number of events at lower redshift. For a larger t_e , all the

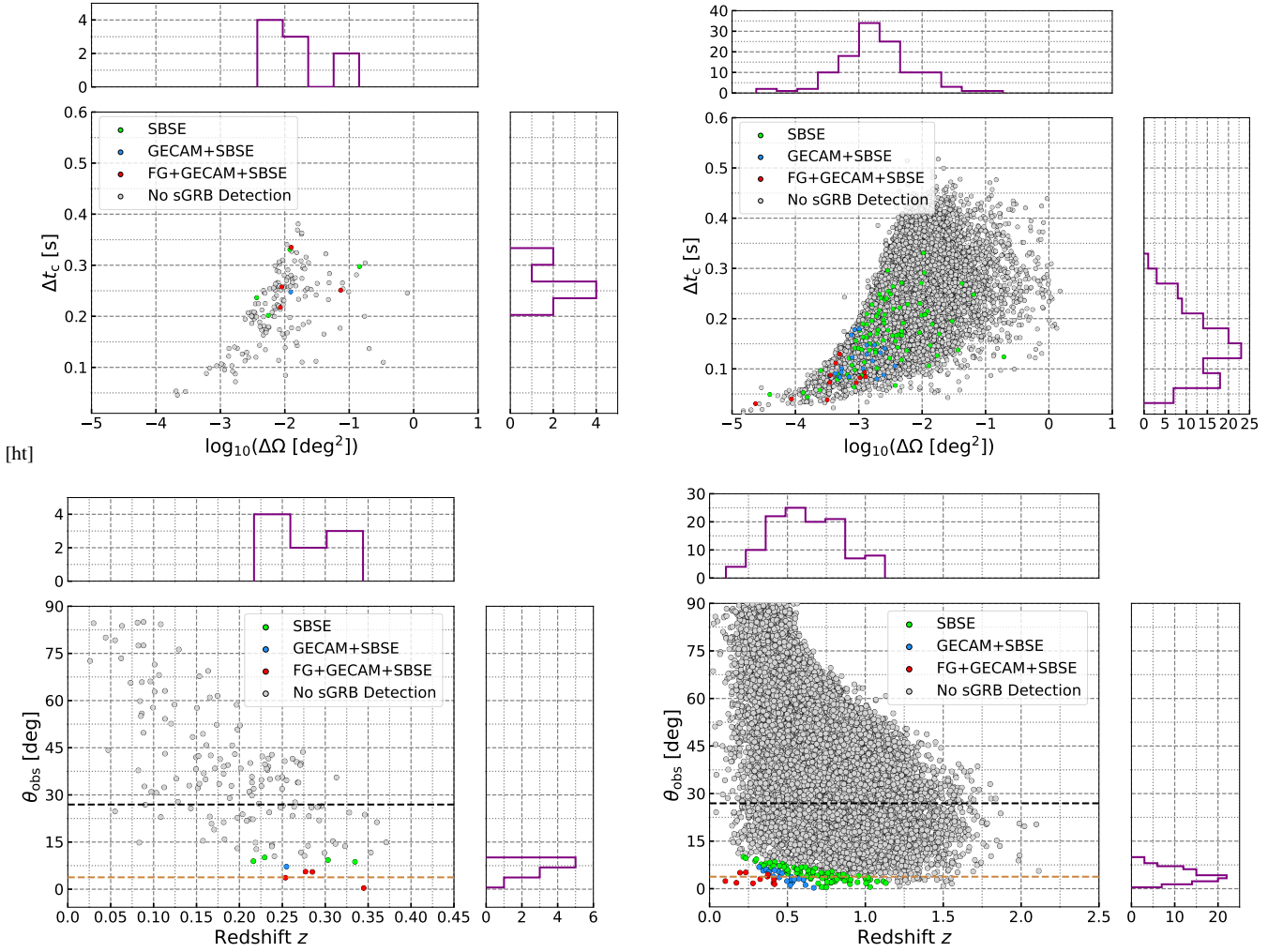


Figure 3. The $\Delta\Omega$ - Δt_c (top panels) and z - θ_{obs} (bottom panels) distributions of our yearly early-warning events in the LN model with $t_e = 1$ d as an example. Left panels are for B-DEC while right panels are for DO-OPT. The dashed horizontal black and brown lines in bottom panels correspond to the fixed values of θ_w and θ_c , respectively (see Sec. 3.1 and Table 1). We plot purple histograms for all the events with joint sGRB detections (i.e., including the green, blue and red circles). Gray circles represent the mergers without sGRB joint detections.

results should behave worse when compared with the values listed in Table 4.

4.2 Characteristics of Multi-messenger Events

As mentioned in Liu et al. (2022a), for BNSs in category (b), B-DEC could reach a localization accuracy of $\Delta\Omega \lesssim 1 \text{ deg}^2$ and timing accuracy around $\Delta t_c \sim 0.1$ s, which is of great use to multi-messenger astronomy. In this subsection, we first compare the $\Delta\Omega$ - Δt_c and z - θ_{obs} distributions of our yearly early-warning samples in the LN model with $t_e = 1$ d for B-DEC and DO-OPT in Fig. 3. Given that different γ -ray detectors vary in the sGRB detection abilities (see Sec. 3.1), we mark all the GW early-warning events with circles in different colors based on whether they can be observed by γ -ray detectors. Specifically, the majority of our early-warning samples denoted by gray circles do not have joint sGRB detections. For the others, we use green circles to denote joint detections that can only be achieved by SBSE, while the blue ones are that can be detected by both SBSE and GECAM. All the joint sGRB detections that can be achieved by the three γ -ray detectors (FG, GACAM and SBSE) are denoted in red circles. In Fig. 3, we further plot all the early-warning events

with joint sGRB detections in purple histograms (i.e., including the green, blue and red circles).

As clearly shown in Fig. 3, one can achieve $\lesssim 1 \text{ deg}^2$ accuracy in localization for almost all events. It is more than adequate for positioning every possible event considering the FoVs of each γ -ray detector (cf. Sec. 4.1). The Δt_c values of B-DEC and DO-OPT are both at $\sim \mathcal{O}(0.1)$ s level. Considering $t_e = 1$ d (or an even larger t_e), such a small timing accuracy will not affect the overall early-warning detections in the wait-for scheme. We also find that the joint sGRB detections are far more likely to be achieved with a lower redshift and a smaller θ_{obs} for the sources. The viewing angle θ_{obs} seems to be the dominating factor in detection abilities, which can be explained well by the exponential decay in Eq. (1).

For the multi-band kilonova detections, we illustrate in Fig. 4 the relationship between the peak AB apparent magnitude of kilonovae and the redshift of the events for our yearly early-warning samples in the LN model with $t_e = 1$ d. Given that there are few GK events in our simulations (see Table 4), an early-warning event with a joint GW-kilonova detection in Fig. 4 is defined as belonging to either the GK samples or the K samples. We again mark all the GW early-warning events from B-DEC and DO-OPT with circles in different

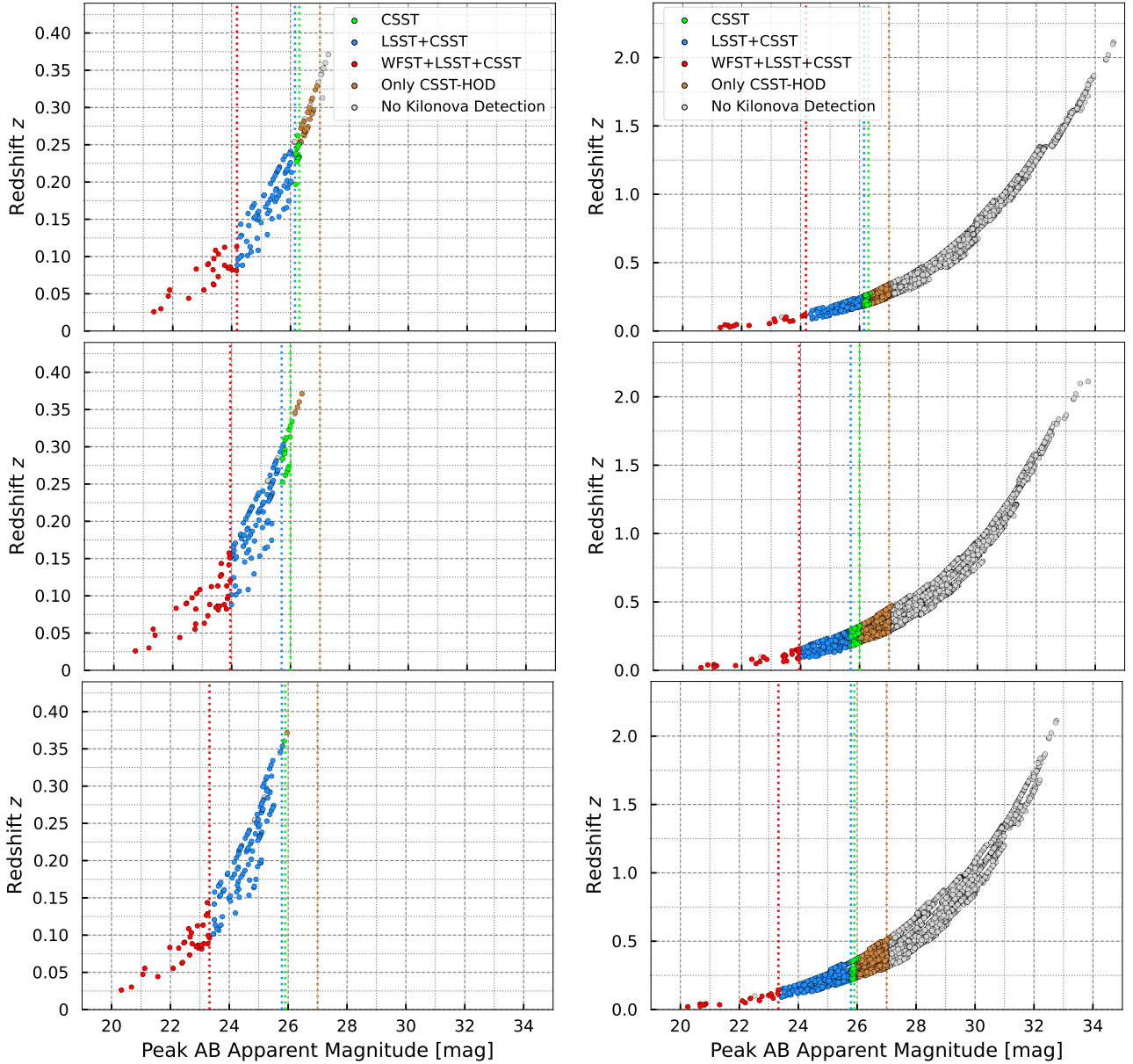


Figure 4. The relationship between the peak AB apparent magnitude of kilonovae and the redshift of the events for our yearly early-warning samples in the LN model with $t_e = 1$ d as an example. Left panels are for B-DEC while right panels are for DO-OPT. Top, middle, and bottom panels correspond to the detections in g , r , and i bands, respectively. Dashed vertical lines with different colors denote the search limiting magnitude m^* of corresponding survey missions (see Sec. 3.2 and Table 2). Circles with different colors represent different joint kilonova detections.

colors based on whether their kilonovae can be detected by survey telescopes. Specifically, we use green circles to denote joint kilonova detections that can only be achieved by CSST, the most sensitive proposed survey telescope except the hypothetical CSST-HOD (see Table 2), while the blue ones are that to be detected by both CSST and LSST. We use red circles to denote the events with kilonovae that can be detected by all three proposed survey missions (WFST, LSST and CSST). The gray circles in Fig. 4 represent the early-warning events without joint kilonova detections. In addition, we use the brown circles to denote events in isolation that can only be seen by CSST-HOD due to its better m^* values in each band (see Sec. 3.2).

Because B-DEC can only detect early-warning sources up to $z \approx 0.45$, the majority of its events are expected to have joint kilonova detections, at least for the CSST. However, it seems rather difficult

to detect most early-warning events of DO-OPT due to their large redshifts, as shown in Fig. 4. Considering the influence of redshift, we see that the i -band observations perform better in Fig. 4, which can be an important consideration in the practical observations, especially for events from DO-OPT.

As mentioned in Sec. 4.1, we no longer need to consider the best searching strategy and FoV influence for our early-warning kilonova detections like previous studies. It is because that with the accuracy of $\Delta\Omega \lesssim 1 \text{ deg}^2$ and $\Delta t_c \lesssim 0.5 \text{ s}$ shown in Fig. 3, such a sufficient early-warning time $t_e = 1 \text{ d}$ (or an even larger t_e) would allow us to locate the optical transients well with survey projects in Table 2. Supposing that there could be HODs to cooperate with B-DEC and DO-OPT in the future—like the CSST-HOD and SBSE-HOD-1 considered in this paper—we can detect more events and more distant sources

using multi-band observations as shown in Fig. 4. Especially, for the events with better location accuracy, more delicate and informative observations are expected for other missions with higher sensitivity rather than larger FoVs as those projects discussed in our work, for an example, the James Webb Space Telescope with an FoV $\sim 100 \text{ arcmin}^2$ (Gardner et al. 2006; Yung et al. 2021).

5 CONCLUSION

In this work, we extend Liu et al. (2022a) to propose a feasible wait-for pattern as a novel detecting mode for various γ -ray detectors and optical survey missions in the near future in synergy with space-borne decihertz GW detectors. Such a methodology is based on the GW early-warning populations of BNS mergers using two space-borne decihertz observatories. The analysis is performed using the method of Fisher matrix. With a sufficient early-warning time $t_e = 1 \text{ d}$ (or an even larger t_e), we point out that one can prepare well in advance for the EM transients after the BNS mergers and no longer needs to consider the FoV discounts and complex searching strategies like in previous studies. We not only give quick assessments of yearly joint sGRB detection rates for different γ -ray detectors and BNS population models, but also report detailed analyses and results on kilonova detections for several survey telescopes with different search limiting magnitudes in g , r , and i bands. We find that DO-OPT has better performances than B-DEC as a whole during an assumed 4-yr mission time, especially for the high-redshift events. Taking the LN population model with $t_e = 1 \text{ d}$ as an example, we present the localization and timing abilities of space-borne decihertz GW observatories and discuss the redshift distributions for various EM and GW synergy observations. Furthermore, given that there might be no overlapping observational time for proposed EM projects and B-DEC/DO-OPT, we have considered some HODs with better sensitivities than the current designs in this work for multi-messenger observations. Note that a specific ground-based EM project should consider the discount due to its maximum detectable sky coverage and the Earth's rotation. But for such a wait-for pattern, we suggest that this discount problem can be partially solved if there are at least two survey telescopes on the different sides of the Earth. In contrast to sGRBs, the relatively long duration of kilonovae will also diminish the discount.

While most research about multi-messenger observations of BNS mergers has focused on the low-latency GW triggers and early warnings from ground-based GW detectors (Hooper et al. 2012; Nitz et al. 2018; Abbott et al. 2019b; Sachdev et al. 2020; Nitz & Dal Canton 2021; Singh et al. 2021; Magee & Borhanian 2022; Borhanian & Sathyaprakash 2022), there are few studies on the realistic detections of BNS merger populations and early warnings with space-borne decihertz GW observatories (Liu & Shao 2022; Liu et al. 2022a). As we have demonstrated in this paper, space-borne decihertz observatories could have a prominent advantage over ground-based GW detectors by gathering enough information from the pre-merger stages of BNS mergers. Decihertz GW observatories can also provide the location and time of the merger in advance to the EM facilities. The $O(0.01) \text{ deg}^2$ localization precision and $O(0.1) \text{ s}$ timing accuracy achieved by decihertz GW detectors will not only increase the joint detection rates for the future EM follow-up projects, but also provide another unprecedented opportunity for analyzing the early evolution of each detectable system, such as the properties of pre- and post-merger precursors as suggested by some observational results and theoretical works (Troja et al. 2010; Li & Yu 2016; Gottlieb et al. 2018; Bromberg et al. 2018; Gottlieb & Loeb 2020; Levinson

& Nakar 2020; Nakar 2020; Wang et al. 2020; Wang & Liu 2021; Sridhar et al. 2021). We leave this to a future study.

In our Monte Carlo simulations, we have adopted a GRB 170817A-like Gaussian jet structure and AT2017gfo-like model to justify whether the simulated mergers could be detected by various γ -ray detectors and optical survey missions. Our results can be used to provide meaningful references and helpful inputs for upcoming EM follow-up projects by exploring the prospects for multi-messenger early-warning detections. We hope that more studies are carried out in the future in order to give more precise predictions of sGRBs and kilonovae with detailed analyses.

ACKNOWLEDGEMENTS

It is a great pleasure to thank Jin-Ping Zhu for his useful advice and comments. This work was supported by the National Natural Science Foundation of China (11975027, 11991053, 11721303), the National SKA Program of China (2020SKA0120300), the Max Planck Partner Group Program funded by the Max Planck Society, and the High-Performance Computing Platform of Peking University. Y.K. acknowledges the Hui-Chun Chin and Tsung-Dao Lee Chinese Undergraduate Research Endowment (Chun-Tsung Endowment) at Peking University.

DATA AVAILABILITY

The data underlying this paper will be shared on a reasonable request to the corresponding author.

REFERENCES

- Abbott B. P., et al., 2017a, *PhRvL*, 119, 161101
- Abbott B. P., et al., 2017b, *ApJL*, 848, L12
- Abbott B. P., et al., 2017c, *ApJL*, 848, L13
- Abbott B. P., et al., 2017d, *ApJL*, 850, L39
- Abbott B. P., et al., 2018, *PhRvL*, 121, 161101
- Abbott B. P., et al., 2019a, *PhRvL*, 123, 011102
- Abbott B. P., et al., 2019b, *ApJ*, 875, 161
- Abbott B. P., et al., 2020, *ApJL*, 892, L3
- Abbott R., et al., 2021, arXiv e-prints, [p. arXiv:2111.03634](https://arxiv.org/abs/2111.03634)
- Abell P. A., et al., 2009, arXiv, [p. arXiv:0912.0201](https://arxiv.org/abs/0912.0201)
- Ade P. A. R., et al., 2016, *A&A*, 594, A13
- Arun K. G., et al., 2022, arXiv, [p. arXiv:2205.01597](https://arxiv.org/abs/2205.01597)
- Becerra R. L., et al., 2021, *MNRAS*, 507, 1401
- Borhanian S., Sathyaprakash B. S., 2022, arXiv, [p. arXiv:2202.11048](https://arxiv.org/abs/2202.11048)
- Bromberg O., Tchekhovskoy A., Gottlieb O., Nakar E., Piran T., 2018, *MNRAS*, 475, 2971
- Bulla M., 2019, *MNRAS*, 489, 5037
- Chen P., et al., 2020, *ApJL*, 889, L6
- Coughlin M., Dietrich T., Kawaguchi K., Smartt S., Stubbs C., Ujevic M., 2017, *ApJ*, 849, 12
- Coughlin M. W., et al., 2020a, *NatCo*, 11, 4129
- Coughlin M. W., et al., 2020b, *MNRAS*, 497, 1181
- Coulter D. A., et al., 2017, *Sci*, 358, 1556
- Cowperthwaite P. S., Berger E., 2015, *ApJ*, 814, 25
- Cowperthwaite P. S., Villar V. A., Scolnic D. M., Berger E., 2019, *ApJ*, 874, 88
- Dichiara S., et al., 2021, *ApJL*, 923, L32
- Domink M., Belczynski K., Fryer C., Holz D. E., Berti E., Bulik T., Mandel I., O'Shaughnessy R., 2013, *ApJ*, 779, 72
- Evans P. A., et al., 2017, *Sci*, 358, 1565
- Gardner J. P., et al., 2006, *SSRv*, 123, 485

- Gehrels N., et al., 2004, *ApJ*, 611, 1005
- Gehrels N., Cannizzo J. K., Kanner J., Kasliwal M. M., Nissanke S., Singer L. P., 2016, *ApJ*, 820, 136
- Ghirlanda G., et al., 2019, *Sci*, 363, 968
- Goldstein A., et al., 2017, *ApJL*, 848, L14
- Gong Y., et al., 2019, *ApJ*, 883, 203
- Gottlieb O., Loeb A., 2020, *MNRAS*, 493, 1753
- Gottlieb O., Nakar E., Piran T., Hotokezaka K., 2018, *MNRAS*, 479, 588
- Götz D., et al., 2015, *PoS, SWIFT10*, 074
- Hjorth J., et al., 2017, *ApJL*, 848, L31
- Hooper S., Chung S. K., Luan J., Blair D., Chen Y., Wen L., 2012, *PhRvD*, 86, 024012
- Ioka K., Nakamura T., 2019, *MNRAS*, 487, 4884
- Isoyama S., Nakano H., Nakamura T., 2018, *PTEP*, 2018, 073E01
- Kalogera V., et al., 2021, arXiv, [p. arXiv:2111.06990](https://arxiv.org/abs/2111.06990)
- Kasen D., Badnell N. R., Barnes J., 2013, *ApJ*, 774, 25
- Kasen D., Metzger B., Barnes J., Quataert E., Ramirez-Ruiz E., 2017, *Natur*, 551, 80
- Kasliwal M. M., et al., 2020, *ApJ*, 905, 145
- Kawaguchi K., Shibata M., Tanaka M., 2020, *ApJ*, 889, 171
- Kawaguchi K., Fujibayashi S., Shibata M., Tanaka M., Wanajo S., 2021, *ApJ*, 913, 100
- Kawamura S., et al., 2021, *PTEP*, 2021, 05A105
- Kilpatrick C. D., et al., 2017, *Sci*, 358, 1583
- Kiziltan B., Kottas A., De Yoreo M., Thorsett S. E., 2013, *ApJ*, 778, 66
- Korobkin O., et al., 2021, *ApJ*, 910, 116
- Lamb G. P., et al., 2019, *ApJL*, 870, L15
- Lattimer J. M., 2012, *ARNPS*, 62, 485
- Lazzati D., Perna R., Morsony B. J., López-Cámara D., Cantiello M., Ciolfi R., Giacomazzo B., Workman J. C., 2018, *PhRvL*, 120, 241103
- Levinson A., Nakar E., 2020, *PhR*, 866, 1
- Li L.-X., Paczynski B., 1998, *ApJL*, 507, L59
- Li S.-Z., Yu Y.-W., 2016, *ApJ*, 819, 120
- Lien A., Sakamoto T., Gehrels N., Palmer D. M., Barthelmy S. D., Graziani C., Cannizzo J. K., 2014, *ApJ*, 783, 24
- Liu C., Shao L., 2022, *ApJ*, 926, 158
- Liu C., Shao L., Zhao J., Gao Y., 2020, *MNRAS*, 496, 182
- Liu C., Kang Y., Shao L., 2022a, arXiv, [p. arXiv:2204.06161](https://arxiv.org/abs/2204.06161)
- Liu M.-X., Tong H., Hu Y.-M., Chan M. L., Liu Z., Sun H., Hendry M., 2022b, *RAA*, 21, 308
- Lyman J. D., et al., 2018, *NatAs*, 2, 751
- Madau P., Dickinson M., 2014, *ARA&A*, 52, 415
- Magee R., Borhanian S., 2022, arXiv, [p. arXiv:2201.11841](https://arxiv.org/abs/2201.11841)
- Margutti R., et al., 2017, *ApJL*, 848, L20
- Mazzali P. A., Sauer D. N., Pastorello A., Benetti S., Hillebrandt W., 2008, *MNRAS*, 386, 1897
- McBrien O. R., et al., 2019, *ApJL*, 885, L23
- Meegan C., et al., 2009, *ApJ*, 702, 791
- Metzger B. D., 2017, *LRR*, 20, 3
- Metzger B. D., Berger E., 2012, *ApJ*, 746, 48
- Metzger B. D., et al., 2010, *MNRAS*, 406, 2650
- Mohite S. R., et al., 2022, *ApJ*, 925, 58
- Mooley K. P., et al., 2018, *Natur*, 554, 207
- Nakar E., 2020, *PhR*, 886, 1
- Nitz A. H., Dal Canton T., 2021, *ApJL*, 917, L27
- Nitz A. H., Dal Canton T., Davis D., Reyes S., 2018, *PhRvD*, 98, 024050
- O'Connor B., et al., 2021, *MNRAS*, 502, 1279
- O'Connor B., et al., 2022, arXiv, [p. arXiv:2204.09059](https://arxiv.org/abs/2204.09059)
- Perley D. A., et al., 2019, *MNRAS*, 484, 1031
- Pian E., et al., 2017, *Natur*, 551, 67
- Preece R. D., Briggs M. S., Mallozzi R. S., Pendleton G. N., Paciesas W. S., Band D. L., 2000, *ApJS*, 126, 19
- Prentice S. J., et al., 2018, *ApJL*, 865, L3
- Rossi E., Lazzati D., Rees M. J., 2002, *MNRAS*, 332, 945
- Rosswog S., Feindt U., Korobkin O., Wu M. R., Sollerman J., Goobar A., Martinez-Pinedo G., 2017, *CQGra*, 34, 104001
- Ryan G., van Eerten H., Piro L., Troja E., 2020, *ApJ*, 896, 166
- Sachdev S., et al., 2020, *ApJL*, 905, L25
- Sathyaprakash B., et al., 2019, *BAAS*, 51, 251
- Savchenko V., et al., 2017, *ApJL*, 848, L15
- Sedda M. A., et al., 2020, *CQGra*, 37, 215011
- Shi D. D., Zheng X. Z., Zhao H. B., Lou Z., Wang H. R., Qian Y., Liu W., Yao D. Z., 2018, *AcASn*, 59, 22
- Singh N., Bulik T., Belczynski K., Askar A., 2021, arXiv, [p. arXiv:2112.04058](https://arxiv.org/abs/2112.04058)
- Song H.-R., Ai S.-K., Wang M.-H., Xing N., Gao H., Zhang B., 2019, *ApJL*, 881, L40
- Sridhar N., Zrake J., Metzger B. D., Sironi L., Giannios D., 2021, *MNRAS*, 501, 3184
- Sun H., Zhang B., Li Z., 2015, *ApJ*, 812, 33
- Tanvir N. R., Levan A. J., Fruchter A. S., Hjorth J., Wiersema K., Tunnicliffe R., de Ugarte Postigo A., 2013, *Natur*, 500, 547
- Troja E., Rosswog S., Gehrels N., 2010, *ApJ*, 723, 1711
- Troja E., et al., 2017, *Natur*, 551, 71
- Troja E., et al., 2018, *MNRAS*, 478, L18
- Troja E., et al., 2019a, *MNRAS*, 489, 1919
- Troja E., et al., 2019b, *MNRAS*, 489, 2104
- Troja E., et al., 2020, *MNRAS*, 498, 5643
- Wanderman D., Piran T., 2015, *MNRAS*, 448, 3026
- Wang J., Liu L., 2021, *Galax*, 9, 104
- Wang J.-S., Peng Z.-K., Zou J.-H., Zhang B.-B., Zhang B., 2020, *ApJL*, 902, L42
- Xie X., Zrake J., MacFadyen A., 2018, *ApJ*, 863, 58
- Yonetoku D., Murakami T., Nakamura T., Yamazaki R., Inoue A. K., Ioka K., 2004, *ApJ*, 609, 935
- Yu J., et al., 2021, *ApJ*, 916, 54
- Yung L. Y. A., Somerville R. S., Finkelstein S. L., Hirschmann M., Davé R., Popping G., Gardner J. P., Venkatesan A., 2021, *MNRAS*, 508, 2706
- Zhang B., 2018, *The Physics of Gamma-Ray Bursts*. Cambridge University Press, [doi:10.1017/9781139226530](https://doi.org/10.1017/9781139226530)
- Zhang B., Mészáros P., 2002, *ApJ*, 571, 876
- Zhang B. B., et al., 2018, *NatCo*, 9, 447
- Zhang D.-L., et al., 2019, *NIMPA*, 921, 8
- Zhu J.-P., Yang Y.-P., Zhang B., Gao H., Yu Y.-W., 2021a, arXiv, [p. arXiv:2110.10468](https://arxiv.org/abs/2110.10468)
- Zhu J.-P., Wu S., Yang Y.-P., Zhang B., Song H.-R., Gao H., Cao Z., Yu Y.-W., 2021b, arXiv, [p. arXiv:2110.10469](https://arxiv.org/abs/2110.10469)
- Zhu J.-P., et al., 2021c, *ApJ*, 917, 24
- de Jaeger T., et al., 2021, *MNRAS*, 509, 3427

This paper has been typeset from a \LaTeX file prepared by the author.